J. Fluid Mech. (2001), *vol.* 426, *pp.* 155–175. Printed in the United Kingdom

The three-dimensional structure of confined swirling flows with vortex breakdown

By FOTIS SOTIROPOULOS AND YIANNIS VENTIKOS†

School of Civil and Environmental Engineering,
Georgia Institute of Technology, Atlanta, GA 30332–0355, USA

(Received 16 February 1998 and in revised form 5 June 2000)

In a recent experimental study, Spohn, Mory & Hopfinger (1998) investigated in detail the flow in a closed cylindrical container with a rotating bottom for Reynolds numbers in the steady and unsteady regimes. Their visualization photographs revealed that the stationary vortex breakdown bubbles, which form along the container axis within a range of governing parameters, are open, with inflow and outflow, and asymmetric at their downstream end. For Reynolds numbers within the unsteady regime, visualizations of the limiting streamlines on the cylindrical wall showed that the Stewartson layer separates asymmetrically along stationary spiral convergence lines that form below the top cover. We study numerically the container flow, by solving the unsteady, three-dimensional Navier–Stokes equations, in order to clarify the origin and elucidate the underlying physics of these complex, three-dimensional flow features. The stationary vortex breakdown bubbles we simulate exhibit all the asymmetries observed in the laboratory. By analysing the Lagrangian characteristics of the calculated flow fields, we explain the origin of these asymmetries, clarify the experimentally documented filling and emptying mechanisms, and show that the flow in the interior of stationary vortex breakdown bubbles exhibits chaotic particle paths. We also show that the spiral separation lines observed by Spohn *et al.* (1998) inside the Stewartson layer at high Reynolds numbers are due to the growth of pairs of counter-rotating, spiral vortices and the interaction of these vortices with the stationary-cover boundary layer.

1. Introduction

The flow in a closed cylindrical container with a rotating lid has been studied experimentally and computationally for more than thirty years. The first experiments by Vogel (1968) and later Ronnenberg (1977) showed that Ekman suction and pumping, induced by the Ekman layers on the rotating and stationary disks, lead to the formation of a concentrated vortex core along the axis. For length-to-radius (H/R) aspect ratios greater than approximately one, there exists a threshold rotational Reynolds number ($Re = \Omega R^2/\nu$, where Ω is the constant angular speed of the lid) above which this vortex core breaks down in the form of one or more on-axis recirculation bubbles. This feature of the flow and the tremendous importance of vortex breakdown in a number of engineering applications (Leibovich 1978; Escudier 1988; Delery 1994) have made the cylindrical container problem a test-bed for theories aimed at elucidating the fundamental aspects of the bubble mode of the phenomenon.

† Present address: Laboratory for Thermodynamics in Emerging Technologies, Swiss Federal Institute of Technology, ETH–Zentrum, Sonneggstrasse 3, Zurich, CH-8092, Switzerland.

The first comprehensive experimental study of the container problem was undertaken by Escudier (1984) who extended the earlier results of Vogel (1968) and Ronnenberg (1977) to a much wider range of Reynolds numbers and aspect ratios. Escudier (1984) visualized the flow in a diametral plane and obtained a series of photographs showing flow patterns with up to three, depending on Re and H/R, on-axis breakdown bubbles. Sorensen (1992) repeated the same experiment over a broader range of rotational speeds than those investigated by Escudier and argued that above a critical Reynolds number, which is well within the unsteady flow regime, the diametral flow becomes highly asymmetric. Spohn, Mory & Hopfinger (1993) studied the structure of vortex breakdown in a container with a free surface and showed that the presence of the free-surface boundary has a profound effect on both the occurrence and location of the breakdown bubbles. Hourigan, Graham & Thompson (1995) focused on the emergence of asymmetric spirals that were observed along the axis prior to the inception of the first vortex breakdown bubble in both Escudier's (1984) and Spohn *et al.*'s (1993) experiments. They argued that the apparent deflection of the dye filament off the axis is an artifact of the visualization technique and not the manifestation of a three-dimensional instability of the flow. Stevens, Lopez & Cantwell (1999) (see also Stevens *et al.* 1996) studied the flow near the onset of the oscillatory instability and found that both steady and unsteady flows can occur within a limited range of Reynolds numbers above the critical level.

The above experiments were conducted by visualizing the flow in a single diametral plane and yielded images of steady breakdown bubbles that are nearly axisymmetric, exhibiting small but clearly distinguishable asymmetries. The asymmetries appear consistently at the downstream end of the bubbles in the form of distinct asymmetric folds (Escudier 1984; Spohn *et al.* 1993; Stevens *et al.* 1996; Fujimura, Koyama & Hyun 1997). Interestingly, both the shape and location of these folds appear to be strikingly stable in all these studies, regardless of the fact that the experiments were conducted by a variety of investigators in individually constructed experimental rigs. The first attempt to investigate the structure of the flow surrounding the breakdown bubbles and explore in detail the origin of their asymmetric features was reported recently by Spohn, Mory & Hopfinger (1998, referred to as SMH hereafter). Their visualization photographs reveal steady breakdown bubbles with the same asymmetric folds, shaped very similarly to those appearing in all earlier experiments, at their downstream end. They also demonstrate that the breakdown bubbles in the container flow are in many respects similar to unsteady bubbles observed in circular diffusers (Sarpkaya 1971; Faler & Leibovich 1977), both being open and asymmetric at their downstream end. SMH also visualized the limiting streamlines (or friction lines) inside the wall boundary layers and showed that for Reynolds numbers within the unsteady regime the cylindrical-wall boundary layer separates asymmetrically along stationary spiral convergence lines. The work of SMH is a major step towards understanding the complexities of confined swirling flows with vortex breakdown. Their findings strongly suggest, for the first time, that the asymmetries of the breakdown bubbles are not artifacts of the visualization technique, as has been argued in the literature (see for instance Stevens *et al.* 1996, 1999), but rather very real flow features. They also show that there is a threshold Reynolds number above which the sidewall Stewartson layer becomes three-dimensional. We should point out, however, that the underlying physics of the very complex flow phenomena discovered by SMH are still not understood.

There have been numerous computational investigations of the container problem using the axisymmetric incompressible Navier–Stokes equations (Pao 1970; Lugt & Haussling 1973, 1982; Dijkstra & Heijst 1983; Lugt & Abboud 1987; Neitzel 1988;

Lopez 1990; Brown & Lopez 1990; Lopez & Perry 1992; Sorensen & Christensen 1995; Watson & Neitzel 1996; Gelfgat, Bar-Yoseph & Solan 1996; Tsitverblit & Kit 1997). All these studies were able to capture the observed in the laboratory evolution of the flow in the $(H/R, Re)$ parameter space with reasonable accuracy (see, for instance, the work of Lopez 1990). In fact, these simulations not only predicted correctly the onset of vortex breakdown but also reproduced the observed location, size, and number of the on-axis breakdown bubbles. As pointed out by SMH, however, the asymmetric features of vortex breakdown, observed consistently in all existing experiments, cannot be predicted by these simulations, which, by assumption, yield closed and perfectly axisymmetric recirculation bubbles.

The objective of this study is to investigate computationally the container problem in order to explain the complex, three-dimensional flow features observed in the laboratory by SMH. In particular, we seek to elucidate the internal topology of stationary vortex breakdown bubbles and explain the origin of their asymmetric features and to identify the mechanisms that cause the sidewall boundary layer to separate asymmetrically at Reynolds numbers in the unsteady regime. We solve the unsteady three-dimensional Navier–Stokes equations, using a second-order-accurate finite-volume numerical method, for two cylinder aspect ratios, $H/R = 1.75$ and 2, and for Reynolds numbers in the steady and unsteady regimes. Using Lagrangian particle tracking, we examine the details of the flow in and around the on-axis stationary breakdown bubbles. We reproduce all the asymmetric features of the flow observed in the visualization images of SMH for Reynolds numbers in the steady regime, provide, for the first time, a comprehensive description of the three-dimensional topology of the bubble-type mode of vortex breakdown, and show that the flow in the interior of steady vortex breakdown bubbles exhibits chaotic particle paths. Our simulations for Reynolds numbers in the unsteady regime, show that the separation lines observed in the experiment are due to the growth of quasi-stationary pairs of counter-rotating spiral vortices inside the sidewall boundary layer. These vortices appear just above the rotating bottom, spread along the cylinder wall, and interact with the stationary-cover boundary layer causing the Stewartson layer to separate asymmetrically. Based on their structure and the findings of previous experiments with related Stewartson-layer-type flows, we argue that the emergence of these vortices in the container flow is the manifestation of the centrifugal instability of the Stewartson layer.

In § 2 we discuss the mathematical formulation of the problem, outline briefly the numerical method, and describe the mesh sensitivity studies we have conducted. In § 3 we compare the results of our computations with the laboratory observations of SMH and discuss the physics of the flow, including the internal topology and dynamics of stationary vortex breakdown bubbles and the three-dimensional features of the wall boundary layers. Conclusions and areas that require further study are presented in § 4.

2. Formulation of the problem and numerical method

Consider a cylinder of radius R and length H filled with an incompressible Newtonian fluid of constant density ρ and kinematic viscosity ν. One endwall of the cylinder is rotated at a constant angular velocity Ω while the opposite endwall is held stationary (see figure 1 *a*). The two non-dimensional parameters that determine the various flow regimes within this cylinder are the aspect ratio, H/R, and the Reynolds number $Re = \Omega R^2/\nu$.

The flow generated by the rotating endwall is governed by the unsteady, incompressible, three-dimensional Navier–Stokes equations. Due to the grid topology employed

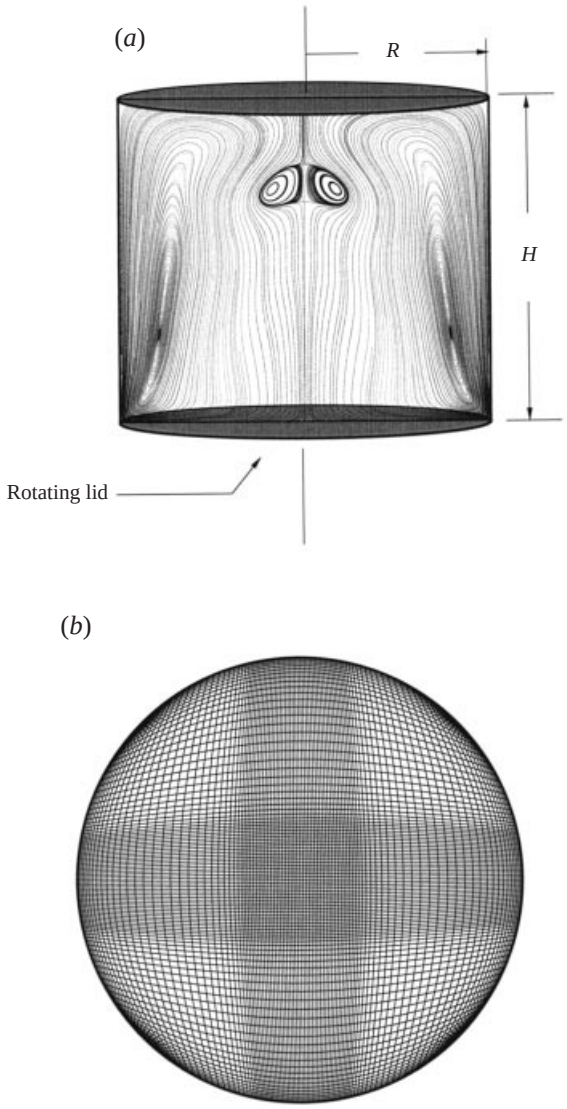

FIGURE 1. Sketch of the cylindrical container configuration (a) and typical cross-sectional computational mesh (b). The calculated diametral streamlines in (a) are for $Re = 1850$ and $H/R = 1.75$ and were constructed by neglecting the azimuthal component of the velocity vector.

in this study (see figure 1 b), the Navier–Stokes equations are formulated in Cartesian coordinates and then transformed into generalized, non-orthogonal, curvilinear coordinates by invoking a partial transformation that retains the Cartesian velocity components as the dependent variables (see Lin & Sotiropoulos 1997 and Sotiropoulos & Ventikos 1998). The transformed equations are discretized on a non-staggered mesh via a conservative finite-volume scheme and integrated in time using a dual (or pseudo) time-stepping artificial compressibility approach enhanced with multigrid acceleration. The numerical method is second-order accurate both in space and time and is described in detail in Sotiropoulos & Ventikos (1998).

All results reported herein have been obtained via time-accurate simulations – that is, even the steady-state flow fields were reached as the time-asymptotic limits of

unsteady computations. For low Reynolds numbers ($Re < 1500$), the calculations were initiated from rest by impulsively spinning up the rotating lid. At higher Reynolds numbers, however, lower-Re flow fields were used for initialization in order to avoid excessive computational times for reaching steady state. For all simulations the physical time step is $\Delta t = 0.02$, which is similar to the time step employed in previous unsteady axisymmetric simulations (Sorensen & Christensen 1995 and Lopez 1990). During a pseudo-time iteration (see Sotiropoulos & Ventikos 1998 for details) the iterative procedure is declared converged when all four residuals (based on the L_1 norm) have been reduced below 10^{-9}. After the initial transients have died out, this level of convergence is achieved within 3 to 6 multigrid iterations per time step.

A typical $X =$ constant cross-section of the computational mesh we employ is shown in figure 1 (*b*). The grid nodes are clustered (using a hyperbolic tangent stretching function) near the outer wall of the cylinder to resolve the sidewall boundary layer. Clustering is also employed around the container axis to ensure sufficient spatial resolution in the vicinity of the vortex breakdown bubbles. The grid nodes in the streamwise direction are distributed uniformly. To investigate the sensitivity of the computed solutions to mesh refinement, we have carried out computations on three, successively finer, meshes: grid A with $100 \times 53 \times 53$ nodes; grid B with $150 \times 73 \times 73$ nodes; and grid C with $150 \times 97 \times 97$ nodes, in the streamwise and transverse directions, respectively. The near-wall grid spacing in these grids was varied from $0.01R$, in grid A, to $0.005R$, in grid C. All subsequently presented results have been obtained on the finest mesh (grid C).

The grid sensitivity of the numerical method was carefully evaluated by comparing solutions obtained on the various meshes in terms of diametral velocity profiles and profiles of axial velocity along the container centreline. These comparisons revealed that, at least for Reynolds numbers in the steady flow regime, even the coarsest mesh employed herein was sufficient for capturing the general features of the flow. We should emphasize, however, that in spite of the very good agreement between coarse and fine mesh solutions, our attempts to employ Lagrangian particle tracking to resolve the internal structure of the breakdown bubbles were not successful on the coarser meshes. Numerical visualization images comparable to those observed in the laboratory (see § 3.1) could only be obtained on meshes that were carefully refined in the vicinity of the vortex breakdown bubble. For instance, for the ($Re = 1492, H/R = 2$) computation (see figures 4–6 below) the Lagrangian characteristics of the breakdown bubble could only be resolved on the B and C meshes, while for the ($Re = 1850, H/R = 1.75$) computation (see figure 2 below) meaningful Lagrangian descriptions of the bubble could only be obtained on the finest mesh (grid C). The sensitivity of the Lagrangian representation of the breakdown bubbles to mesh refinement is attributed to the fact that, as we show in § 3.2 below, the flow in the interior of the bubble exhibits chaotic particle paths.

To verify the ability of the numerical method to capture the general features of the flow, we compare in table 1 calculated locations and sizes of the on-axis vortex breakdown bubbles, for Reynolds numbers in the steady regime, with available experimental data. The computed bubble-defining parameters are in good overall agreement with the data.

3. Results

3.1. *Three-dimensional topology of stationary vortex breakdown bubbles*

To alleviate uncertainties regarding the possible role of the visualization technique in producing deceptive asymmetries, SMH employed a variety of techniques to visualize

		l/H		s/H		h/H			
H/R	Re	Comp.	Exp.	Comp.	Exp.	Comp.	Exp.	Bubble	Ref.
1.75	1850	0.2	0.19	0.116	0.108	0.137	0.126	—	SMH
2	1492	0.323	0.34	0.064	0.06	0.041	0.041	—	Escudier (1984)
2	1854	0.21	0.21	0.176	0.16	0.113	0.113	1	Escudier (1984)
		0.464	0.52*	0.081	0.07*	0.02	0.019	2	
2	2100	0.175	0.18	0.105	—	0.117	—	1	Fujimura *et al.* (1997)
		0.386	—	0.128	—	0.093	—	2	

TABLE 1. Comparison of the computed (Comp.) results with experimental (Exp.) data: l is the distance along the axis from the centre of the top cover to the upstream fixed point of the bubble; s is the axial distance between the upstream and downstream fixed points of the bubble; and h is the maximum half-width of the bubble, measured radially from the axis. An asterisk implies that the data could not be determined with certainty from the available flow visualization images.

the same breakdown bubble for a container with $H/R = 1.75$ at $Re = 1850$. As seen in figures 2(*a*) and 2(*b*), the various techniques produced stationary breakdown bubbles that are open, with both inflow and outflow and distinct asymmetric folds at their downstream end. Note, however, that although both images reveal the same overall asymmetries, the precise shape and size of the bubble appear to depend somewhat on the specific tracer injection technique (SMH).

To construct streakline images that can be directly compared with flow visualization photographs, we release passive particles from a disk centred around the container axis at an axial location just upstream of the breakdown bubble. The three-dimensional particle trajectories are computed using a fourth-order Runge–Kutta method in conjunction with a tri-linear spatial interpolation scheme. Figures 2(*c*) and 2(*d*) show two different visualizations of the computed breakdown bubble for $H/R = 1.75$ and $Re = 1850$. The first image (figure 2*c*) corresponds to a transient bubble and was constructed using an instantaneous velocity field, while the second image (figure 2*d*) is the final steady-state solution. To obtain a bubble like the one shown in figure 2(*c*), we introduced a numerical perturbation by interpolating the steady-state solution obtained on grid B to grid C and integrating the governing equations in time until a new steady-state solution is reached on this finer mesh. After advancing the governing equations over a time interval corresponding to four lid revolutions (approximately 600 time steps), in order to smooth out high-frequency errors introduced by the interpolation, we began monitoring the temporal evolution of the breakdown bubble. The image shown in figure 2(*c*) was obtained after approximately ten lid rotations, from the start of the fine mesh simulation, and it is representative of the bubble shapes observed during the early stages of the transient computation. The final steady-state solution, shown in figure 2(*d*), was achieved after approximately 25 lid rotations from the start of the calculation. Both images reveal that, in close agreement with the observations of SMH, the computed bubbles are open and asymmetric at their downstream end. Interestingly, there are differences between the transient and steady-state bubbles that are similar to those observed among various visualization techniques in the experiment of SMH. In fact, the transient bubble is similar to the experimental bubbles shown in figure 2(*a*), while the steady-state image is more similar to that shown in figure 2(*b*). Note in particular the similarity between the computed and observed shapes of the asymmetric folds for each case. This level of

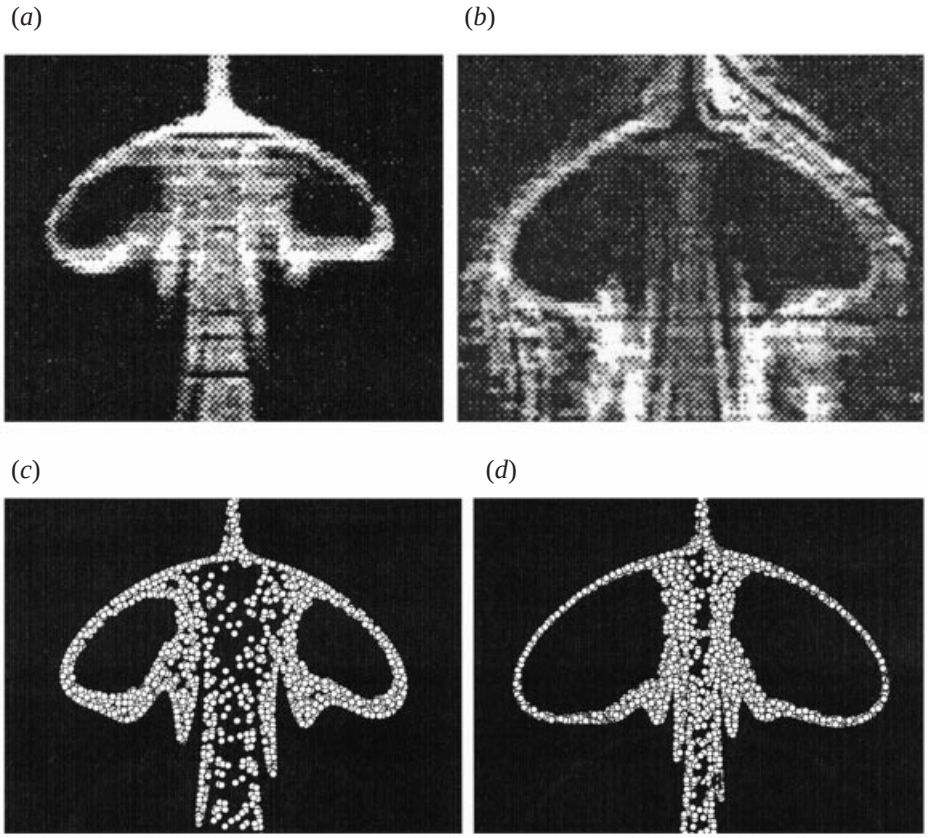

FIGURE 2. Vortex breakdown bubbles observed in the laboratory (by SMH) and calculated for $Re = 1850$, $H/R = 1.75$. (*a*) Flow visualization with electrolytic powder particles released from a solder wire on the stationary cover. (*b*) Flow visualization with electrolytic powder particles released from a solder wire on the cylinder wall (reproduced with permission from SMH). (*c*) Calculated image of a typical bubble during the transient stages of a simulation on grid C. The flow field on this mesh was initialized by interpolating the steady-state solution from the coarser grid B. The image shown was obtained after simulating 10 lid rotations. (*d*) Final steady-state breakdown bubble on grid C obtained after 25 lid rotations. The calculated images were constructed by computing the three-dimensional trajectories of particles released from points along concentric circles located at $X/R = 1.52$ (the radius of the outermost circle is $0.004R$ and along each circle the particles were distributed in an axisymmetric manner). The trajectory of each particle is stored as a sequence of points that mark the position of the particle at every instant in time. The resulting markers for all trajectories are visualized by blanking out those markers that do not fall within a very thin diametral sheet whose thickness is comparable to that of the laser sheet used in the experiment.

agreement with the experimental observations suggests that the inconsistencies among the experimental images could be due to small disturbances introduced by a specific tracer injection technique. This conjecture is consistent with the well-known extreme sensitivity to upstream disturbances of vortex breakdown in diffusers (see Sarpkaya 1995 for a recent discussion).

To further elucidate the internal structure of steady breakdown bubbles, SMH reported a sequence of diametral plane images showing the temporal progression of tracers in and around the bubble for $H/R = 1.75$ and $Re = 1850$. Figure 3 shows several of these images that depict the formation of the asymmetric folds as well as the filling and emptying of the bubble from its downstream end. A similar sequence of

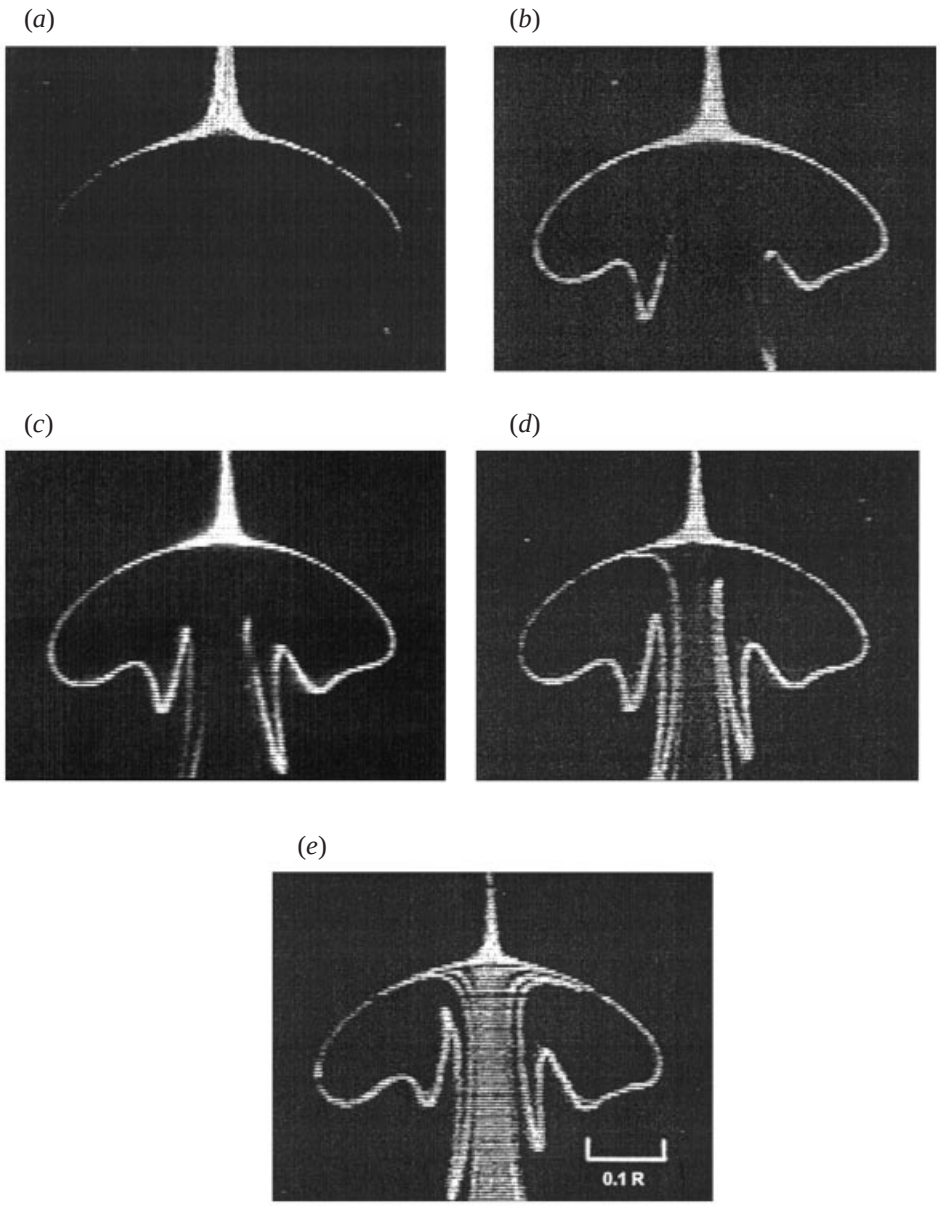

FIGURE 3. Progression in time of electrolytic powder particles in and around the breakdown bubble for $Re = 1850$ and $H/R = 1.75$ (tracers were released from the solder wire on the stationary cover). Elapsed time increases from (*a*) to (*e*). Reproduced with permission from SMH.

images constructed from our numerical solutions is shown in figure 4. However, rather than showing our results for $H/R = 1.75$ and $Re = 1850$, which produce images that are practically identical to those shown in figure 3, we show the steady-state solution for $H/R = 2$ and $Re = 1492$. In spite of the expected differences in the shape and size of the calculated and observed breakdown bubbles, this comparison demonstrates that there are defining structural characteristics of the bubble-type mode of vortex breakdown that do not depend on a specific aspect ratio or Reynolds number.

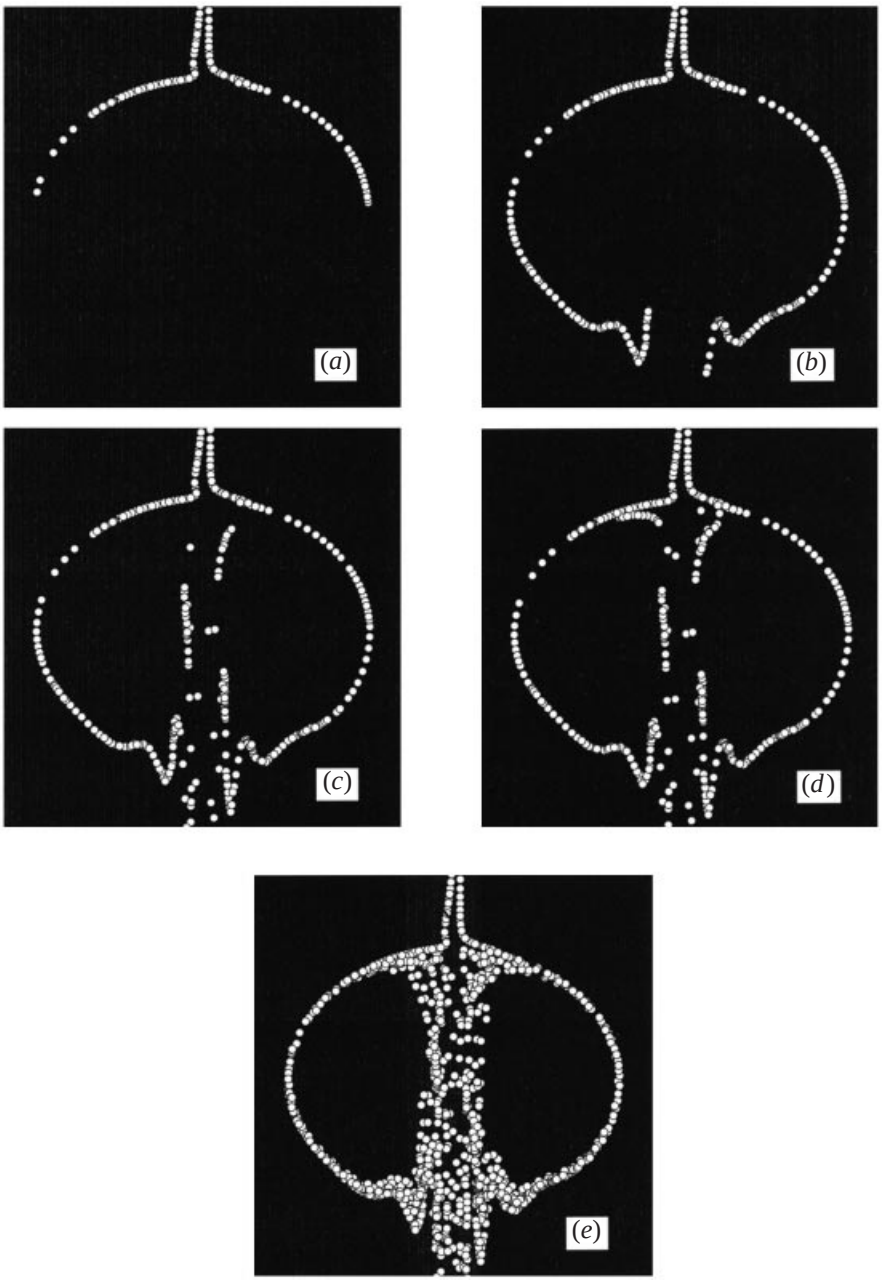

FIGURE 4. Calculated progression in time of particles around the breakdown bubble for $Re = 1492$ and $H/R = 2$. The particles were released axisymmetrically from equally spaced points along a circular rake centred around the axis. The radius of the rake is $0.004R$ and its centre is located upstream of the bubble at $X = 1.52R$. Elapsed time increases from (a) to (e).

During the initial stage of evolution of the computed streak surfaces (figure 4 a), the particles begin to diverge away from the axis into two branches that form the left and right sides of the bubble. Small asymmetries begin to develop during the very early stages of the bubble formation just upstream of the point of radial

divergence. Furthermore, the particles are not equally distributed within the right and left branches of the bubble. Their distribution is especially heterogeneous in the left branch, which consists of an initial segment containing a large number of densely packed particles followed by a segment with significantly fewer particles. Identical trends are also present in the corresponding experimental image shown in figure 3(*a*). During the second stage of the bubble development (see figures 3*b* and 4*b*), the particles continue their progression along the two branches and begin to converge radially inward to form the downstream side of the bubble. As the particles progress toward the container axis, asymmetric folds begin to appear. Comparison between the observed and calculated streaks shows that, in spite of the anticipated quantitative differences due to aspect ratio and Reynolds number, the overall shapes of the folds shown in figures 3(*b*) and 4(*b*) are very similar to each other. The progression of the streak surfaces shown in figures 3(*c, d*) and 4(*c, d*) reveals that particles enter the bubble from its downstream end and begin to move axially upwards. Just before reaching the top of the bubble, they turn sharply away from the axis and move towards the two sides. Figure 4(*e*), which corresponds to a 'fully developed' particle distribution, reveals that there are two asymmetric areas within the bubble that remain free of particles for the duration of the simulated time interval. This feature is consistent with the observations of SMH, see figure 3(*e*), and points to the existence of an asymmetric toroidal region in the interior of the bubble (see figure 5).

In order to clarify the three-dimensional structure of the bubble and explain its asymmetric features, we plot in figure 5 the three-dimensional particle trajectories that were used to construct figure 4(*e*). To also visualize the internal toroidal region, this figure includes the trajectories of a few additional particles that were released from points located within the core of the two empty areas in figure 4(*e*). For clarity, particles that enter the bubble are coloured blue while those that spiral around it are coloured red. As seen in figure 5, the paths of particles initially located on the upstream slender cylindrical filament kink abruptly and begin to spiral around the axis along trajectories of increasing radius. The initiation of the spiralling motion is not axisymmetric, even though the particles were initially released in a perfectly axisymmetric manner. Most of the blue particles in figure 5 cluster together to form a narrow spiral ribbon that retains its coherency as it moves about the axis. On the other hand, the spiral trajectories of adjacent red particles spread continuously away from each other in the azimuthal direction, thus forming the front side of a spherical streak surface. Further downstream all spiral trajectories converge radially inward toward the axis and the spherical streak surface closes to form a bubble-like structure. In this region, the blue and red trajectories define a spiral-in saddle point (see figure 7.7 in Jackson 1991). For the sake of clarity, the temporal integration of the particle trajectories in figure 5 has been continued only up until the point when the blue particles in the interior of the bubble reach its upstream end (corresponding to the two-dimensional image shown in figure 4*d*). Continuation of the integration beyond this point results in a very complicated three-dimensional image that would be very hard to interpret.

The fate of the blue particles at subsequent times becomes clear in figure 6, which shows a sequence of instantaneous trajectories constructed by releasing particles along a segment of the container axis very near to the stationary endwall ($1.99 < X/R < 2.00$). For axisymmetric vortex breakdown, such particles should remain on the axis and stagnate at the upstream end of the bubble. Figure 6, however, reveals that the formation of the bubble is initiated by a small radial deflection of the on-axis filament and its subsequent deformation, following an abrupt kink, into a spiral configuration

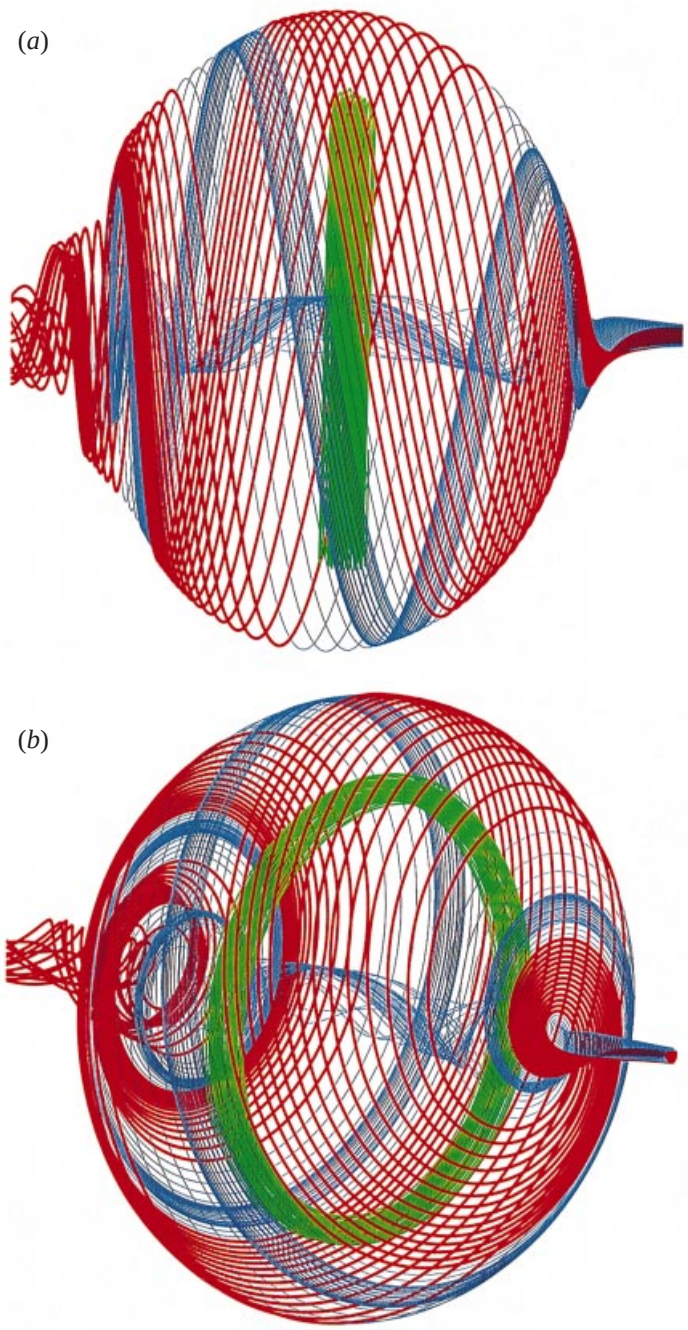

FIGURE 5. Views of three-dimensional particle trajectories in and around the breakdown bubble for $Re = 1492$ and $H/R = 2$. The particles were released axisymmetrically from the same locations as in figure 4. Blue particles enter the bubble, red particles move around it, and green particles define typical toroidal trajectories in the interior of the bubble.

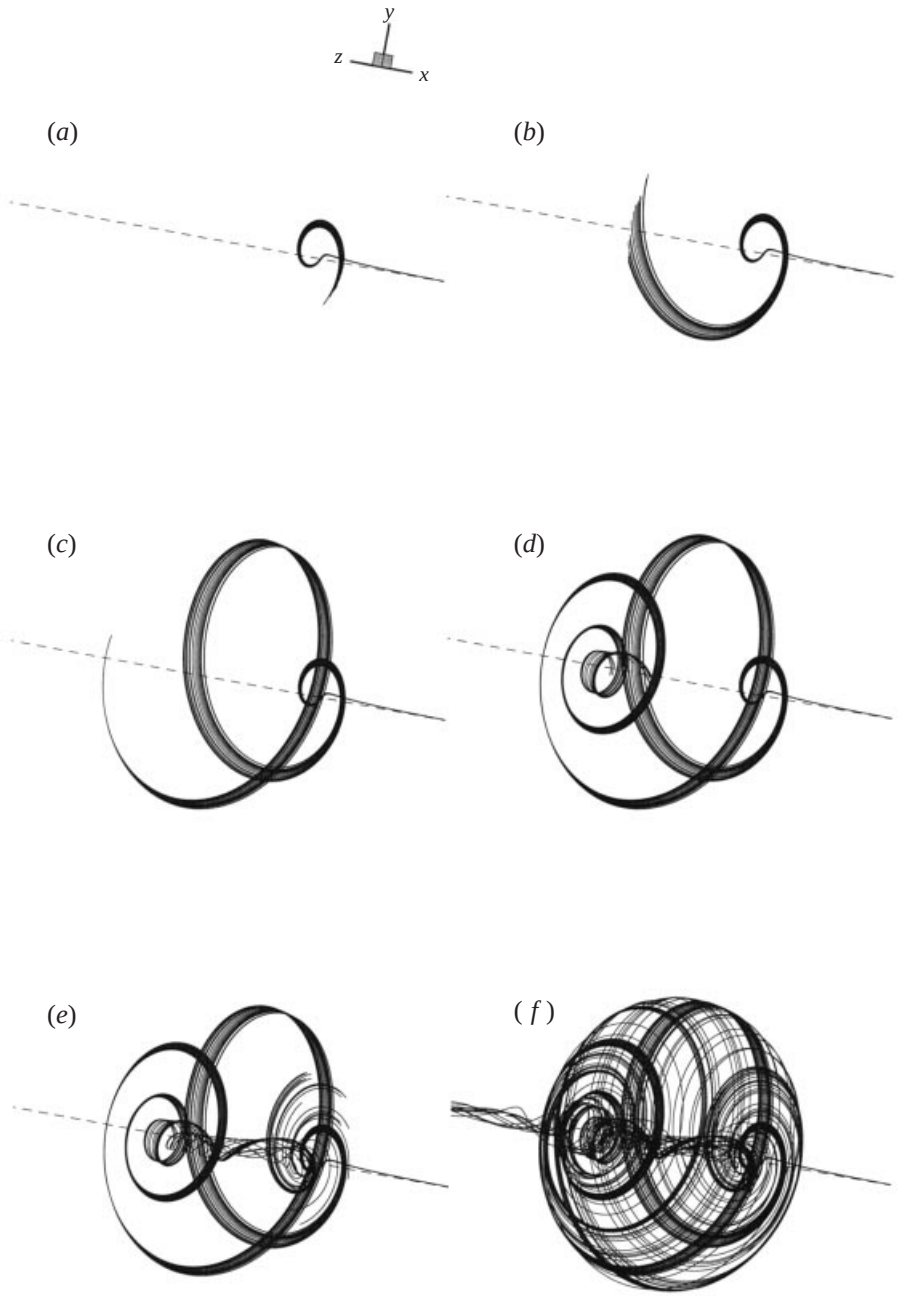

FIGURE 6. Progression in time of trajectories of particles released from a straight segment on the container axis near the centre of the stationary wall ($1.99 < X/R < 2.00$, $Y = Z = 0$) for $Re = 1492$ and $H/R = 2$. Elapsed time increases from (a) to (f).

(see figure 6 a, b). The evolution of the spiral filament is consistent with the motion of the blue spiral ribbon in figure 5. Figure 6, however, illustrates more clearly the filling and emptying of the breakdown region through the downstream spiral-in saddle point. It also reveals that at the upstream end of the bubble the (radially) outward spiralling interior (originating from the spiral-in saddle) and exterior (originating from

the deflected on-axis filament) trajectories define a spiral-out saddle point (Jackson 1991). Notice that interior particles diverge radially away from the spiral-out saddle point and perform several revolutions along the periphery of the bubble as they move downstream and converge once again towards the spiral-in saddle through which they entered initially. After reaching there, particles were observed to either exit the bubble, by spiralling downstream along the axis, or repeat for several times the above described cycle (spiralling upstream near the axis and then downstream along the surface of the bubble) before they too exit through the spiral-in saddle. These highly complex particle trajectories (see § 3.2 below) lead to a 'fully developed' image of the breakdown region that closely resembles an 'axisymmetric bubble' with a spiral tail emanating from its 'open' downstream end. The sequence in figure 6, however, clearly shows that in this case the breakdown process is initiated in a manner identical to a spiral mode. It is the subsequent evolution of the spiral filament, which is compressed in the radial and axial directions and contracts into the bubble, along with the formation of the toroidal region in the interior of the bubble (see figure 5) that give rise to an 'axisymmetric-like' structure.

Figures 5 and 6 help us to explain all the asymmetric features observed in the two-dimensional images shown in figures 3 and 4. The abrupt deflection of the cylindrical filament away from the axis and the initiation of the spiralling motion are responsible for the asymmetries during the early stages of the bubble formation at its upstream end (see figures 3 *a* and 4 *a*). The azimuthal clustering of most of the particles that define the upstream cylindrical filament along a narrow spiral streak surface explains why both branches of the bubble consist of discrete segments of varying particle density. This heterogeneous particle distribution, which as seen in figures 3 and 4 is evident at all stages of the bubble evolution, is the result of the motion of the blue spiral ribbon in and out of a diametral visualization plane. The asymmetric folds at the downstream end of the bubble in figures 3 and 4 (*b–e*) are caused by very complex topology of the trajectories in the vicinity of the spiral-in saddle point. Finally, the areas in the interior of the bubble that in figures 3 and 4 remain free of particles are occupied by toroidal trajectories such as those shown in figure 5.

The stationary vortex breakdown bubble shown in figures 5 and 6 (*f*) exhibits a number of features that suggest significant structural similarities with bubbles observed in circular diffusers. Sarpkaya (1971) and Faler & Leibovich (1977) reported visualization photographs of bubbles whose upstream side appears axisymmetric, but their rear is open and asymmetric. Interestingly, their photographs suggest that the rear side of the bubble is tilted (see also the discussion by Faler & Leibovich 1977), a feature which is clearly evident in figure 5(*a*). Both studies reported that the filling and emptying of the bubble occurs simultaneously through its downstream end. Faler & Leibovich (1977) also reported that a frequently observed feature of the bubble mode was the temporary appearance of dye on the axis in the interior of the bubble. Their visualization photographs reveal a dye filament that appears similar to the 'blue' filament in the interior of the calculated bubble as shown in figure 5. The presence of the toroidal region in the interior of the bubble, shown in figure 5, is also in accordance with the early observations of Sarpkaya (1971) and the more recent measurements by Brücker & Althaus (1992). It is important to emphasize, however, that there is an important difference between the bubble-type breakdown observed in these experiments and that simulated herein for the container case. In all these studies, the entire breakdown region was found to be quite unsteady oscillating back and forth along the diffuser axis (Sarpkaya 1971; Faler & Leibovich 1977; Brücker & Althaus 1992) and the simultaneous emptying and filling of the

bubble was attributed to unsteady periodic fluctuations in the wake region (Sarpkaya 1971; Faler & Leibovich 1977; Brücker & Althaus 1992). For the container flow the present results demonstrate that there exists a range of Reynolds numbers within which the breakdown bubbles are steady, open, and asymmetric and exhibit most of the structural characteristics observed in diffuser geometries. Similar conclusions were also reached by SMH.

3.2. *Chaotic particle paths in stationary vortex breakdown bubbles*

As we have already pointed out, there have been several numerical studies of the axisymmetric container problem that succeeded in reproducing general features of the experimental flow (Lopez 1990; Sorensen & Christensen 1995; Gelfgat *et al.* 1996; Tsitvertblit & Kit 1998; etc.). Yet the complex Lagrangian characteristics of the breakdown bubbles we uncovered herein demonstrate clearly that these axisymmetric solutions are in fact fundamentally different from the real flow fields visualized in the laboratory. Leibovich (1984) was the first to suggest this some fifteen years ago, by pointing out that steady solutions of the axisymmetric Navier–Stokes equations with reversed flow regions do exist but cautioned that such solutions need not be close to the nearly axisymmetric flows observed in the experiments. Holmes (1984) elaborated further on Leibovich's arguments and envisaged a scenario via which even a very small, time-periodic, asymmetric forcing may be sufficient to fundamentally alter the internal dynamics of a steady, axisymmetric vortex breakdown bubble. Holmes specifically argued that such a mode could destabilize the downstream fixed hyperbolic point of the axisymmetric flow, making the bubble accessible to upstream fluid. He further speculated that the perturbed flow inside the breakdown bubble must be spatially chaotic. The Lagrangian studies we presented above confirm the general scenario described by Holmes and clarify the topological features of the perturbed fixed hyperbolic points. We should emphasize, however, that Holmes discussed the structure of a time-periodic, unsteady flow whereas our findings, along with the available laboratory experiments, suggest that the same general emptying and filling mechanisms are at work even in stationary breakdown bubbles. To explore Holmes's conjecture regarding the chaotic nature of the flow inside a three-dimensional vortex breakdown bubble, we examine herein the sensitivity of particle trajectories to initial conditions. Figure 7 depicts the temporal evolution of the inter-particle distance for a pair of particles that were initially released from 'arbitrarily' close positions (an initial separation length of $10^{-7}R$ was specified) within the breakdown region in the vicinity of the axis. As seen in figure 7, the two particles diverge exponentially in time as they circulate inside the bubble, eventually becoming completely uncorrelated from each other ($s/S_{\max} \rightarrow 1$). This extreme sensitivity of particle trajectories to initial conditions within real-life breakdown bubbles establishes the existence of at least one positive Lyapunov exponent and proves the chaotic nature of the flow (Aref 1984; Ottino 1989). Obviously this very important feature cannot be captured by axisymmetric simulations, which by definition yield steady flows with integrable dynamics.

Detailed numerical and experimental investigations of the chaotic dynamics of particle paths within steady vortex breakdown bubbles are currently under way and their results will be reported in future communications. A small sample of these results can be found in Sotiropoulos & Ventikos (2000).

3.3. *Three-dimensional features of the wall boundary layers*

To explore the origin of the asymmetries of the vortex breakdown bubbles, SMH visualized the limiting streamlines along the cylinder wall and the stationary cover

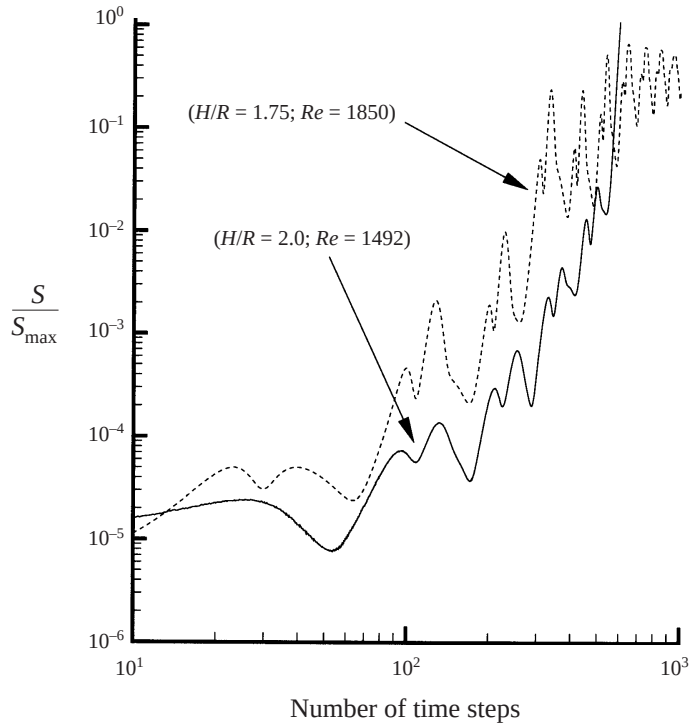

FIGURE 7. Temporal variation of the distance, s, between two particles initially located $10^{-7}R$ apart. For each case, the particles are released in the interior of the bubble within the cylindrical near-axis filament. The three-dimensional bubbles are those shown in figures 2(*d*) and 4(*e*). The reference length scale, $S_{\max}$, is the width of the breakdown region, which represents the maximum possible separation distance for two particles confined within the breakdown bubble. Log-log scale is used to demonstrate the exponential divergence of the particles.

using the electrolytic precipitation method. They showed visualization photographs for two Reynolds number, $Re = 1850$ (in the steady regime) and $Re = 6000$ (well within the unsteady regime for $H/R = 1.75$).

For $Re = 1850$, SMH found that the Stewartson layer remains attached until it reaches the upper corner of the container where it separates, to satisfy the imposed no-flux condition, and spirals radially inward towards the centre of the stationary cover. Interestingly, however, they observed that the sidewall flow does not enter the stationary, cover Ekman layer axisymmetrically, but rather forms distinct azimuthal clusterings (figure 8*a*). Our steady-state computations for $Re = 1850$ reproduce this experimental finding (see the limiting streamline comparisons in figure 8), thus pointing to the conclusion that three-dimensional disturbances must be present inside the sidewall boundary layer. These disturbances render the stationary-cover Ekman layer three-dimensional and introduce non-axisymmetric modes on the vortex core that emanates from its centre, which are presumably responsible for the three-dimensional structure of the vortex breakdown bubbles. The nature of the three-dimensional bifurcation of a steady axisymmetric flow and the exact Reynolds number at which such a bifurcation first occurs, are not at present known.

Since the curvilinear grids we employ herein introduce fixed non-axisymmetric modes, the mechanism that causes the break of axial symmetry cannot be addressed by our numerical approach and will be left as a topic for future work. In fact this

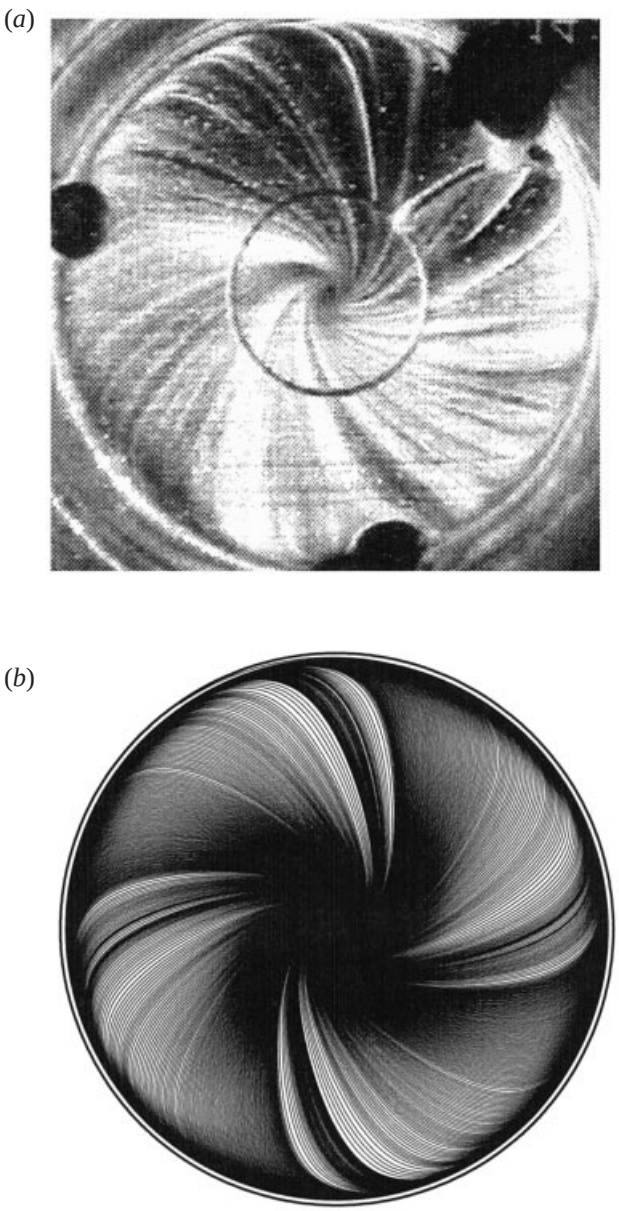

FIGURE 8. (*a*) Visualized (SMH) and (*b*) computed limiting streamlines along the stationary cover for $Re = 1850$ and $H/R = 1.75$. To construct (*b*), streamlines were released axisymmetrically from equally spaced points along a circular rake of radius $r = 0.99R$ located at $X = 1.99R$. Experimental image is reproduced with permission from SMH.

is a rather perplexing issue since, as we have already discussed, steady axisymmetric solutions of the Navier–Stokes equations, which capture some Eulerian features of the laboratory flow reasonably well, do exist and have been reported in the literature (Lopez 1990). Yet the experiments of SMH appear to suggest that, at least for the range of Reynolds numbers they considered, such perfectly axisymmetric flows may not be realizable experimentally. This apparent discrepancy between laboratory experiments and the solutions of the axisymmetric Navier–Stokes equations may be due

to the fact that the latter simulate the flow in an ideal (disturbance-free) environment. The laboratory flow, on the other hand, always takes place in a slightly imperfect container due to unavoidable non-axisymmetric disturbances arising from, among others, geometrical, thermal, and dynamical experimental imperfections (Stevens *et al.* 1996). The presence of such imperfections would result in a small but finite non-axisymmetric forcing imposed on the laboratory flow at all Reynolds numbers – in our simulations, we impose a fixed, non-axisymmetric forcing through the curvilinear mesh we employ. Our calculations in conjunction with the work of SMH establish firmly the fact that such a forcing does not simply act to distort somewhat an otherwise axisymmetric flow, but rather excites three-dimensional modes that modify the structure of the wall boundary layers even in the steady flow regime.

Figures 9 (*a*) and 9 (*b*) depict the visualized (by SMH) and calculated, respectively, limiting streamlines along the cylinder wall for $Re = 6000$. The calculated limiting streamlines exhibit two very pronounced spiral separation lines below the stationary cover. Two more lines (a total of four separation lines are found in our computations) are also present at the diametrically opposite side of the cylindrical wall, which has been blanked out for clarity – the origins of these two lines are nonetheless visible near the left vertical side of figure 9 (*b*). The SMH flow visualization photograph, figure 9 (*a*), shows clearly one spiral separation line whose location and overall orientation correspond well with the computed line 1 in figure 9 (*b*). It also shows a second, albeit somewhat faded, spiral line that is parallel to the main line and located closer to the stationary cover. Although the experimental photograph is not of sufficient clarity (recall that SMH illuminated only a portion of the cylindrical surface) to establish conclusively the existence of this second line, its presumed location agrees well with the computed line 2 in figure 9 (*b*). In fact, superimposing figures 9 (*a*) and 9 (*b*) shows that the computed lines 1 and 2 practically coincide with the corresponding lines in the experimental photograph. We should point out that SMH did not comment on the existence of this second line, neither did they report the total number of separation lines they observed along the circumference of the cylinder.

To elucidate the mechanism that gives rise to these spiral separation lines, we show in figure 9 (*c*) the structure of two instantaneous iso-surfaces of constant radial velocity component (U_r), corresponding to a positive and a negative U_r value, respectively. The existence of well-defined spiral interfaces between the positive and negative iso-surfaces along with the streaky structure of the limiting streamlines in figure 9 (*b*), suggest the presence of four pairs of counter-rotating spiral vortices inside the sidewall boundary layer. These vortices emanate just above the rotating lid, spread along the cylinder wall and interact with the stationary-cover boundary layer. The interaction causes the fluid in the upwash region between adjacent vortices to be ejected away from the wall before reaching the stationary cover, thus leading to the formation of the asymmetric separation lines observed by SMH. Since the Stewartson layer loses stability to disturbances in the form of counter-rotating vortex pairs, the nature of this three-dimensional instability appears to be of centrifugal type. Calculated circulation profiles, not shown herein, show that the potential for centrifugal instability certainly exists according both to the Rayleigh (1916) criterion and to the criterion proposed by Floryan (1991) for boundary layers developing on curved walls (see also Hart 1971). Furthermore, the development of spiral vortices inside Stewartson layers has been documented in previous experimental investigations of related centrifugally unstable flows (Weidman 1976; Escudier, Bornstein & Maxworthy 1982; Hart & Kittelman 1996).

It is important to emphasize that although at $Re = 6000$ the flow is well within the

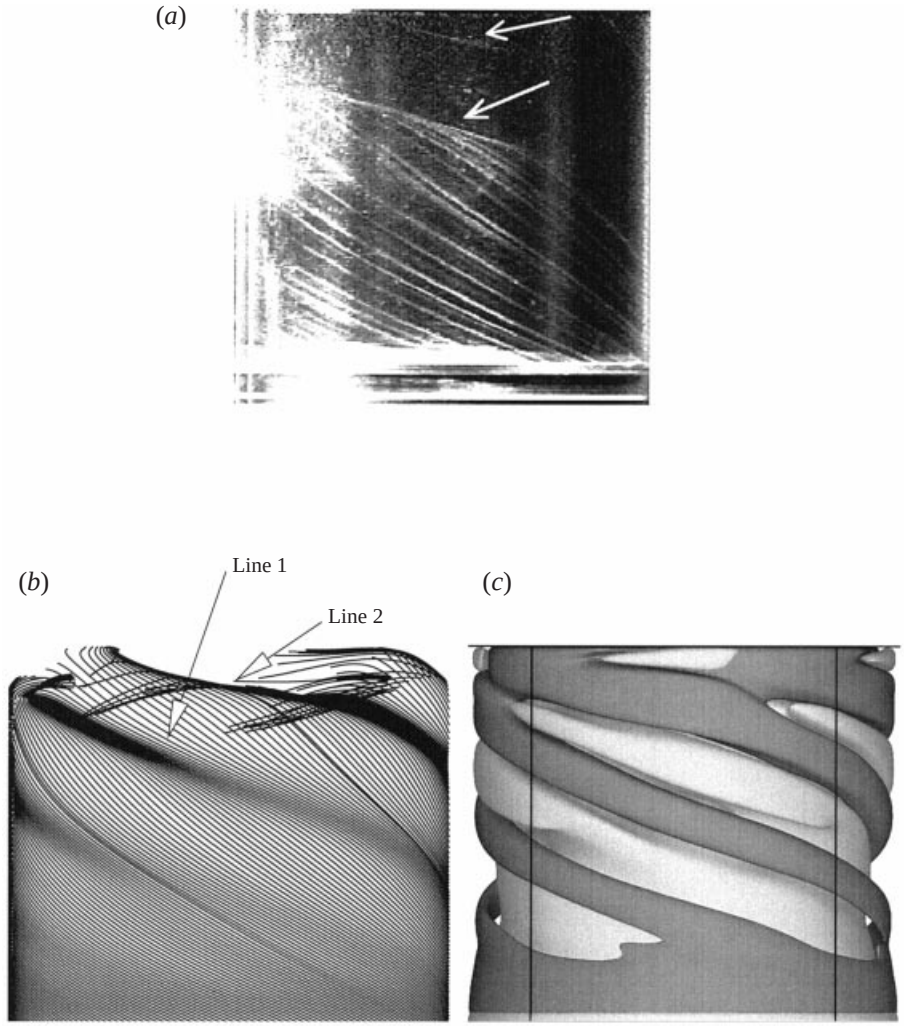

FIGURE 9. (*a*) Visualized (SMH) and (*b*) calculated near-wall streamlines and (*c*) instantaneous iso-surfaces of constant radial velocity component, showing pairs of counter-rotating spiral vortices along the cylinder wall ($Re = 6000$ and $H/R = 1.75$). (*a*) The experimental image (reproduced with permission from SMH) has been obtained by illuminating only a portion of the cylinder wall. The two arrows mark the locations of the separation lines. The lower arrow is from the original photograph of SMH. The top arrow has been included by us. (*b*) Streamlines were computed by distributing axisymmetrically 200 particles along the cylinder circumference at $X/R = 0.1$ and $r = 0.99R$. For clarity, streamlines on the opposite side of the cylinder have been blanked out. (*c*) $U_r = -0.002, 0.001$ (dark and light surfaces correspond to negative and positive values, respectively).

unsteady regime, the spiral vortical structures in our computations reach (after initial transients have decayed) a quasi-steady state. Video animations of the computed solutions show significant unsteady fluctuations of the flow in the interior of the container while the location of the cylindrical wall spirals remains essentially frozen in time. This finding is supported by the observations of SMH, who reported that the location and shape of the friction lines along the cylinder wall at $Re = 6000$ are remarkably stable in time, even though the interior flow is highly unsteady. It is also broadly consistent with the experiments of Hart & Kittleman (1996) who visualized

quasi-stationary spiral vortices within the centrifugally unstable Stewartson layer in a related cylindrical geometry.

4. Summary and closing remarks

We have obtained numerical solutions of the unsteady, three-dimensional, Navier–Stokes equations to examine the asymmetries observed in laboratory models of the flow in an enclosed cylinder driven by a rotating endwall. The accuracy of our solutions was established by comparing numerically generated streakline images of stationary vortex breakdown bubbles, which form along the container axis for certain values of container aspect ratio and Reynolds number, with the visualization photographs of SMH. We have shown that all asymmetric features of the bubbles observed in the laboratory can be reproduced numerically with reasonable accuracy. By analysing the three-dimensional topology of the computed particle paths, we clarified the origin of the asymmetric folds at the downstream end of the bubbles and explained the filling and emptying mechanisms observed in the laboratory. We also showed that the trajectories of particles originating from arbitrarily close initial positions diverge exponentially in time as they recirculate in the interior of the bubble. This finding proves that the flow in the interior of stationary vortex breakdown bubbles is spatially chaotic and places the container problem among a handful of experimentally realizable, three-dimensional flow fields that can be used to study stirring due to chaotic advection. Although chaotic advection plays a critical role in a variety of problems in engineering and geophysics, its in-depth study, particularly in three-dimensional flows of technological importance, has been hindered by the lack of test-bed flow fields (Aref 1984; Ottino 1989; Cartwright, Feingold & Piro 1996; etc.). The numerically simulated vortex-breakdown flow fields provide a unique test-bed for investigating various aspects of the phenomenon in the steady, transitional (steady-to-unsteady), and unsteady flow regimes.

In accordance with the laboratory observations of SMH, we also found that the asymmetric features of the stationary vortex breakdown bubbles along the axis are linked to asymmetries that originate inside the stationary-cover Ekman layer and the sidewall Stewartson layer. Our computations have also helped clarify the origin of the spiral separation lines inside the Stewartson layer observed in the laboratory (just below the rotating lid) for Reynolds numbers in the unsteady regime. They are due to the emergence of counter-rotating pairs of spiral vortices, which emanate just above the rotating lid, spread across the cylinder wall, and cause the sidewall boundary layer to separate asymmetrically, within the upwash regions of adjacent vortices, before reaching the stationary cover. We argued that the growth of these vortices is a manifestation of the centrifugal instability of the Stewartson layer. We should point out, however, that there are several aspects concerning the structure of the wall boundary layers in the laboratory flow that are not at present understood. These include the mechanism that leads to the experimentally documented three-dimensional bifurcation of the flow in the steady regime, the link between the boundary layer asymmetries in the steady regime and the spiral vortices that appear to characterize the unsteady regime, and the possible role of the spiral vortices in triggering the onset of unsteady flow (see Tsitverblit & Kit 1998 for some interesting comments on this issue). Combined experiments and three-dimensional computations will be needed to tackle these issues, whose understanding is critical for further elucidating the complexities of confined swirling flows.

The computations were performed on the Cray T-90 supercomputer of the San Diego Supercomputer Centre and the Silicon Graphics Origin 2000 system of the Office of Information Technology at the Georgia Institute of Technology. We are especially grateful to A. Spohn, M. Mory, and E. J. Hopfinger for kindly providing us with a copy of their paper well before it was published. In particular, we wish to thank Andreas Spohn for several very illuminating email communications.

REFERENCES

Aref, H. 1984 Stirring by chaotic advection. *J. Fluid Mech.* **143**, 1–21.

Brown, G. L. & Lopez, J. M. 1990 Axisymmetric vortex breakdown. Part 2. Physical mechanisms. *J. Fluid Mech.* **221**, 553–576.

Brücker, C. & Althaus, W. 1992 Study of vortex breakdown by particle tracking velocimetry (PTV). Part 1: Bubble-type vortex breakdown. *Exps. Fluids* **13**, 339–349.

Cartwright, J. H. E., Feingold, M. & Piro, O. 1996 Chaotic advection in three-dimensional unsteady incompressible laminar flow. *J. Fluid Mech.* **316**, 259–284.

Delery, J. M. 1994 Aspects of vortex breakdown. *Prog. Aerospace Sci.* **30**, 1–59.

Dijkstra, D. & Heijst, G. J. F. van 1983 The flow between two finite rotating disks enclosed by a cylinder. *J. Fluid Mech.* **128**, 123–154.

Escudier, M. P. 1984 Observations of the flow produced in a cylindrical container by a rotating endwall. *Exps. Fluids* **2**, 189–196.

Escudier, M. P. 1988 Vortex breakdown: Observations and explanations. *Prog. Aerospace Sci.* **25**, 189–229.

Escudier, M. P., Bornstein, J. & Maxworthy, T. 1982 The dynamics of confined vortices. *Proc. R. Soc. Lond.* A **382**, 335–360.

Faler, J. H. & Leibovich, S. 1977 Disrupted states of vortex flow and vortex breakdown. *Phys. Fluids* **20**, 1385–1400.

Faler, J. H. & Leibovich, S. 1978 An experimental map of the internal structure of vortex breakdown using a laser Doppler anemometer. *J. Fluid Mech.* **86**, 313–335.

Floryan, J. M. 1991 On the Görtler instability of boundary layers. *Prog. Aerospace Sci.* **28**, 235–271.

Fujimura, K., Koyama, H. S. & Hyun, J. M. 1997 Time-dependent vortex breakdown in a cylinder with a rotating lid. *Trans. ASME: J. Fluids Engng* **119**, 450–453.

Gelfgat, A. Yu., Bar-Yoseph, P. Z. & Solan, A. 1996 Stability of confined flow with and without vortex breakdown. *J. Fluid Mech.* **311**, 1–36.

Hart, J. E. 1971 Instability and secondary motion in a rotating channel. *J. Fluid Mech.* **45**, 341–351.

Hart, J. E. & Kittelman, S. 1996 Instabilities of the sidewall boundary layer in a differentially driven rotating cylinder. *Phys. Fluids* **8**, 692–696.

Holmes, P. 1984 Some remarks on chaotic particle paths in time-periodic, three-dimensional swirling flows. *Contemp. Maths* **28**, 393–404.

Hourigan, K., Graham, L. J. W. & Thompson, M. C. 1995 Spiral streaklines in pre-vortex breakdown regions of axisymmetric swirling flows. *Phys. Fluids* **7**, 3126.

Jackson, E. A. 1991 *Perspectives of Nonlinear Dynamics 2*. Cambridge University Press.

Leibovich, S. 1978 The structure of vortex breakdown. *Ann. Rev. Fluid Mech.* **10**, 221–246.

Leibovich, S. 1984 Vortex stability and breakdown: Survey and extension. *AIAA J.* **22**, 1192–1206.

Lin, F. & Sotiropoulos, F. 1997 Assessment of artificial dissipation models for three-dimensional, incompressible flow solutions. *Trans. ASME: J. Fluids Engng* **119**, 314–324.

Lopez, J. M. 1990 Axisymmetric vortex breakdown. Part 1. Confined swirling flow. *J. Fluid Mech.* **221**, 533–552.

Lopez, J. M. & Perry, A. D. 1992 Axisymmetric vortex breakdown. Part 3. Onset of periodic flow and chaotic advection. *J. Fluid Mech.* **234**, 449–471.

Lugt, H. & Abboud, M. 1987 Axisymmetric vortex breakdown with and without temperature effects in a container with a rotating lid. *J. Fluid Mech.* **179**, 179–200.

Lugt, H. & Haussling, H. J. 1973 Development of flow recirculation in a rotating tank. *Acta Mech.* **18**, 255–272.

LUGT, H. & HAUSSLING H. J. 1982 Axisymmetric vortex breakdown in rotating fluid within a container. *Trans. ASME: J. Appl. Mech.* **49**, 921–922.

NEITZEL, G. P. 1988 Streak-line motion during steady and unsteady axisymmetric vortex breakdown. *Phys. Fluids* **31**, 958–960.

OTTINO, J. M. 1989 *The Kinematics of Mixing: Stretching, Chaos, and Transport*. Cambridge University Press.

PAO, H.-P. 1970 A numerical computation of a confined rotating flow. *Trans. ASME: J. Appl. Mech.* **37**, 480–487.

RAYLEIGH, LORD 1916 On the dynamics of revolving fluids. *Proc. R. Soc. Lond.* A **93**, 148–154 (reprinted in *Scientific Papers 6*, p. 447). Cambridge University Press.

RONNENBERG, B. 1977 Ein selbstjustierendes 3-Komponenten-Laserdoppleranemometer nach dem Vergeichsstrahlvefahren, angewandt auf Untersuchungen in einer stationären zylinder- symmetrischen Drehströmung mit einen Rückströmgebiet. *Max-Planck-Institut für Strömungsforschung, Göttingen, Bericht* 19.

SARPKAYA, T. 1971 On stationary and travelling vortex breakdowns. *J. Fluid Mech.* **45**, 545–559.

SARPKAYA, T. 1995 Vortex breakdown and turbulence. *AIAA Paper*. 95-0433.

SORENSEN, J. N. 1992 Visualization of rotating fluid flow in a closed cylinder. Rep. AFM 92-06, Department of Fluid Mechanics, Technical University of Denmark.

SORENSEN, J. N. & CHRISTENSEN, E. A. 1995 Direct numerical simulation of rotating fluid flow in a closed cylinder. *Phys. Fluids* **7**, 764–778.

SOTIROPOULOS, F. & VENTIKOS, Y. 1998 Transition from bubble-type vortex breakdown to columnar vortex in a confined swirling flow. *Intl J. Heat Fluid Flow* **19**, 446–458.

SOTIROPOULOS, F. & VENTIKOS, Y. 2000 Three-dimensional steady vortex breakdown in laboratory models of confined swirling flows. *2000 ASME Fluid Engineering Summer Conference*, Paper FED SM 2000-11203.

SPOHN, A., MORY, M. & HOPFINGER, E. J. 1993 Observations of vortex breakdown in an open cylindrical container with rotating bottom. *Exps. Fluids* **13**, 70–77.

SPOHN, A., MORY, M. & HOPFINGER, E. J. 1998 Experiments on vortex breakdown in a confined flow generated by a rotating disk. *J. Fluid Mech.* **370**, 73–99 (referred to herein as SMH).

STEVENS, J. L., CELIK, Z. Z., CANTWELL, B. J., & LOPEZ, J. M. 1996 Experimental study of vortex breakdown in a cylindrical swirling flow. *Joint Institute for Aeronautics and Acoustics* Rep. JIAA TR 117, Department of Aeronautics and Astronautics, Stanford University.

STEVENS, J. L., LOPEZ, J. M. & CANTWELL, B. J. 1999 Oscillatory flow states in an enclosed cylinder with a rotating endwall. *J. Fluid Mech.* **389**, 101–118.

TSITVERBLIT, N. & KIT, E. 1998 On the onset of unsteadiness in confined vortex flows. *Fluid Dyn. Res.* **23**, 125–152

VOGEL, H. U. 1968 Experimentelle Ergebnisse über die laminare Strömung in einem zylindrischen Gehäuse mit darin rotierender scheibe. *Max-Planck-Institut für Strömungsforschung, Göttingen, Bericht* 6.

WATSON, J. P. & NEITZEL, G. P. 1996 Numerical evaluation of a vortex-breakdown criterion. *Phys. Fluids* **8** 3063–3071.

WEIDMAN, P. D. 1976 On the spin-up and spin-down of a rotating fluid. Part 2. Measurements and stability. *J. Fluid Mech.* **77**, 709–735.